Computational Geosciences
https://doi.org/10.1007/s10596-023-10216-3

ORIGINAL PAPER

An integrated framework for optimal monitoring and history matching in CO_2 storage projects

Dylan M. Crain[1] · Sally M. Benson[1] · Sarah D. Saltzer[1] · Louis J. Durlofsky[1]

Received: 17 November 2022 / Accepted: 20 April 2023

Abstract
Monitoring is an important component of geological carbon storage operations because it provides data that can be used to estimate key quantities such as CO_2 plume location. The design of the monitoring strategy is complicated, however, because the monitoring plan must be established prior to the availability of extensive flow data. In this work, we present and apply a framework that integrates monitoring well optimization and (subsequent) history matching. The monitoring well optimization entails finding the locations of monitoring wells such that, with the data acquired at those locations, the expected uncertainty reduction in a particular flow quantity is maximized. This optimization requires the simulation of a large set of prior models, though these simulations need only be performed once for a given injection scenario. Once the monitoring wells are in place and CO_2 injection begins, history matching is performed using the monitoring data. This is accomplished here using an ensemble smoother with multiple data assimilation. The overall framework is applied to variogram-based geomodels that are representative of an actual storage project under development in the USA. Two injection scenarios are considered with two different (synthetic) 'true' models, which provide the observed data. History matched models are constructed using data from both optimally located and heuristically placed monitoring wells. Posterior uncertainty, evaluated in terms of the cumulative distribution function for a metric related to plume extent over the ensemble of history matched models, is shown to be minimized through use of optimized monitoring wells. These results demonstrate the importance of optimizing the monitoring plan, and the degree of uncertainty reduction that can be realistically achieved.

Keywords Carbon capture and Storage · Monitoring well · Optimization · Reservoir simulation · Data assimilation

1 Introduction

Subsurface storage of CO_2 in deep saline aquifers represents a promising strategy for achieving large reductions in greenhouse gas emissions to the atmosphere. Monitoring is an essential aspect of any storage operation, as it can identify leakage and provide information on the location of the CO_2 plume. Although monitoring is conducted over many decades, an initial monitoring plan must be defined when CO_2 injection begins. This poses challenges because the storage aquifer geology is highly uncertain at this point, yet monitoring well locations and types must nonetheless be in place.

In this paper, we describe an overall strategy for determining the 'optimal' locations of monitoring wells and for history matching using pressure and saturation data as they are collected during CO_2 injection. The monitoring well optimization is accomplished using the general approach described in [21]. This procedure requires simulation of an ensemble of prior geological realizations. Monitoring well locations are then determined such that the expected uncertainty reduction is maximized (under Gaussian assumptions on the data). Once CO_2 injection is underway, the monitoring wells provide pressure and saturation data. History matching using these observed data is accomplished through use of an ensemble smoother with multiple data assimilation, ES-MDA [7]. Our procedures are demonstrated on models

✉ Dylan M. Crain
cooper96@stanford.edu

Sally M. Benson
smbenson@stanford.edu

Sarah D. Saltzer
sarah.saltzer@stanford.edu

Louis J. Durlofsky
lou@stanford.edu

[1] Department of Energy Science and Engineering, Stanford University, 94305 Stanford, CA, USA

Published online: 23 July 2023

corresponding to an actual sequestration project now being planned for the Illinois basin in the USA.

Many previous investigations have addressed monitoring and history matching for CO_2 storage operations. Here we discuss studies that are most relevant to our work. History matching using multilevel pressure time-series data was performed for a carbon sequestration pilot project in Illinois, USA [20]. The history matching process was heuristic, though the results demonstrated the utility of assimilating multilevel pressure data. Geophysical data from electromagnetic and seismic surveys, as well as satellite images, have also been used for history matching in carbon sequestration [1, 16, 23]. According to [9, 13], well-based pressure and saturation measurements, along with seismic surveys, provide the most informative data in practice.

Recent studies involving data assimilation have often applied some type of ensemble-based history matching. ES-MDA, in particular, has been widely used in CO_2 storage studies [2, 6, 22]. ES-MDA is more expensive than some other ensemble-based methods because the data assimilation computations are repeated several times (there are typically 4–10 assimilation steps). For this reason, recent work has focused on reducing computational cost by modifying the algorithm [6, 10, 22] or by using surrogate flow models to approximate expensive forward flow simulations [12, 14, 16, 23, 24].

There has also been a substantial amount of work on determining monitoring plans for CO_2 storage projects. Monitoring wells can be used for different objectives, including detecting leakage and identifying the plume location. Although our interest here is in minimizing uncertainty in the plume location, existing work in both areas is relevant to our investigation. In several previous studies, monitoring well locations and sensor types were specified heuristically, and the post-history matching uncertainty reduction for each scenario was assessed [4, 5, 14, 25]. This procedure can be iterated manually to achieve further reduction in expected posterior uncertainty. Optimal experimental design has also been applied in this setting [11, 26]. Particle swarm optimization (PSO) was used in [3] to find the optimum monitoring well locations that minimized the uncertainty in a particular metric. However, in order to reduce computational costs, samples were drawn from a set of prior results instead of being generated through history matching. A more formal approach was presented in [21], where monitoring wells were placed such that a metric quantifying posterior uncertainty was minimized.

In this work, we combine ideas from some of the studies noted above to define an overall monitoring and history matching framework. The locations of a predefined number and type of monitoring wells are optimized using a variant of the procedure presented in [21]. This requires the simulation of an ensemble of prior models intended to capture the range of prior geological uncertainty. Then, under the assumption of Gaussian prior and posterior flow statistics, the optimal monitoring well locations can be determined without conducting additional simulations. The objective of the monitoring well optimization is to maximize the degree of uncertainty reduction in a quantity related to plume location. Once the storage project is in operation, history matching (ES-MDA) is performed using pressure and saturation measurements from the monitoring wells. The framework is applied to models based on those for a storage operation being planned for Illinois, USA [17]. The performance of the methodology will be demonstrated for different synthetic 'true' models and different injection strategies.

This paper proceeds as follows. In Section 2, we describe the computational approaches for monitoring well optimization and history matching. Next, in Section 3, the aquifer model used in this study is presented. Numerical results are then provided for several cases, and the reduction in uncertainty achieved using optimized monitoring well locations is compared to that using heuristic designs. Finally, in Section 4, we summarize our findings and give suggestions for future work in this area.

2 Optimization of monitoring well locations and history matching procedure

Our goal in this study is to maximize uncertainty reduction in carbon storage operations by applying history matching using data from monitoring wells. The amount of uncertainty reduction that can be achieved is dependent on the number of monitoring wells, their locations, and the type of data they provide. A key challenge in this setting is that the permitting procedure requires a monitoring plan to be established before any CO_2 is injected, and thus before any flow data are collected. This means that one or more monitoring well locations must be determined based only on a prior understanding of the subsurface geology.

The workflow applied here is illustrated in Fig. 1. This framework involves two steps – monitoring well optimization and history matching. We assume that all monitoring wells are drilled prior to injection. Thus the two steps, which will now be described, are sequential. The procedure could be modified to include the addition of monitoring wells during the injection stage, but this is not considered here.

2.1 Monitoring well location optimization

In this work, the monitoring scheme is optimized using a modified version of the strategy described in Sun and Durlofsky [21]. In that study, a data-space inversion procedure was applied, and the goal was to provide posterior data predictions, e.g., CO_2 plume location at a particular time. Here our

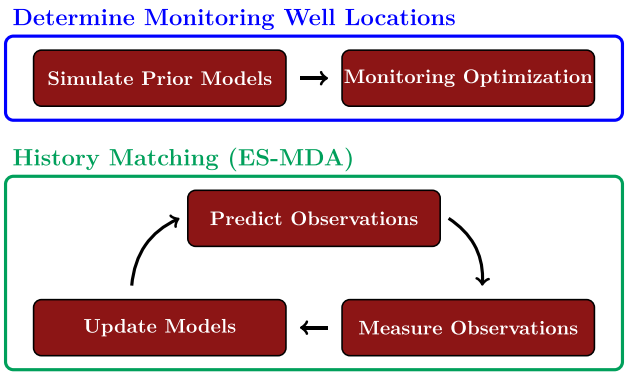

Fig. 1 Workflow for CO_2 monitoring and history matching. Monitoring well locations are determined in the first step, and history matching is then performed as CO_2 is injected over time

goal is to construct posterior (history matched) geomodels. The monitoring well optimization step, however, is essentially the same regardless of whether the history matching entails a data-space or a model-based procedure.

The vector containing the uncertain aquifer model parameters is represented by $\mathbf{m} \in \mathbb{R}^{N_m \times 1}$. Here $N_m = 2N_b$, where N_b is the number of grid blocks in the geomodel. The two geological parameters in each grid block correspond to porosity and permeability. Only a single value is required for permeability because we set $k_x = k_y$ and take $k_z = \alpha k_x$, where α is a specified parameter (here k_x, k_y, and k_z denote directional permeabilities). The aquifer models in this work are based on those in Okwen et al. [17], in which porosity and permeability are uncorrelated. Thus, we do not prescribe any correlation between these two sets of parameters in the models used here.

The forward simulation model is represented as

$$\mathbf{d}_f = \mathbf{g}(\mathbf{m}), \tag{1}$$

where $\mathbf{g}$ denotes the flow simulation and $\mathbf{d}_f \in \mathbb{R}^{N_f \times 1}$ represents simulation results. Our intent is to determine the optimal monitoring well locations such that, at a prescribed (future) time, the uncertainty reduction in a quantity of interest (QoI) will be maximized. For specificity, here this QoI is a measure of the plume extent after 20 years of CO_2 injection. Data up to this time are referred to as 'historical' data (even though no data have yet been collected) and are denoted by $\mathbf{d}_h \in \mathbb{R}^{N_h \times 1}$, where N_h is the number of observations. Data corresponding to the QoI are denoted $\mathbf{d}_p \in \mathbb{R}^{N_p \times 1}$, where N_p is the number of QoI. The data vector $\mathbf{d}_f$ can be viewed as a concatenation of these two sets of data, i.e., $\mathbf{d}_f = [\mathbf{d}_h^T, \mathbf{d}_p^T]^T$.

We proceed by first simulating a set of N_r prior geological models, intended to represent our prior knowledge of the subsurface. In this study we set $N_r = 350$. This will provide a large set of prior data vectors – specifically, $(\mathbf{d}_f)_i$, $i = 1, \ldots, N_r$, each of which is comprised of $(\mathbf{d}_h)_i$ and $(\mathbf{d}_p)_i$, $i = 1, \ldots, N_r$. The goal of the first-stage optimization is to determine the monitoring well locations such that the measured data, when used for history matching, minimize an appropriate metric over the set of prior models.

Monitoring wells are assumed to extend vertically through the entire storage aquifer, with areal locations defined by their (i, j) locations on the simulation grid. Monitoring wells can contain multiple transducers, each of which provides pressure data, along their length. We denote the number of pressure transducers on each well by N_t, and treat each transducer as if it is located in the center of the grid block. Each monitoring well is thus defined by $2 + N_t$ design variables (i and j areal locations and N_t vertical locations). The full set of N_w monitoring wells is denoted by $\mathbf{y} \in \mathbb{N}^{N_y \times 1}$, where $N_y = N_w \times (2 + N_t)$.

In our setup, the goal is to maximize uncertainty reduction in a plume-location metric after 20 years of injection. We assume that pressure data are measured every 3 months at the pressure transducer locations, and that CO_2 saturation is measured along the monitoring well once per year. This is accomplished in practice using a saturation logging tool [8].

The actual observations will contain error due to imprecision in the measurements, along with model error, though the latter may be difficult to quantify. We denote the observed data as $\mathbf{d}_{obs} \in \mathbb{R}^{N_h \times 1}$, with $\boldsymbol{\epsilon} \in \mathbb{R}^{N_h \times 1}$ the measurement error. Here $\boldsymbol{\epsilon}$ is assumed to be normally distributed with mean $\mathbf{0}$ and covariance $C_D \in \mathbb{R}^{N_h \times N_h}$.

Strandli et al. [20] cited a pressure measurement error of about 1 kPa (0.001 MPa), while Sun and Durlofsky [21] applied a pressure error of 0.1 MPa, which includes some amount of model error. The latter study used a saturation error of 0.02. Here we use a pressure error of 10.34 kPa (1.5 psi), which is between those used in [20] and [21], and a saturation error of 0.02, as in [21]. The model error contribution could be adjusted in cases where this component can be accurately quantified.

The $\mathbf{d}_p$ portion of $\mathbf{d}_f$ in our case corresponds to a scalar QoI, which will be used in the monitoring well optimization problem (note the QoI must be a scalar quantity in our optimization framework). Here this quantity is the volume of CO_2 beyond a given target region after 20 years of injection. The target region here is taken to be a volume corresponding to $n \times n \times n_p$ blocks around the injection well(s). Here $n = 5$ or 7, and n_p is the number of layers in which the well is perforated. Further details (and illustrations) will be provided in Section 3.

This QoI, now denoted by J, is given by

$$J = \sum_{i \notin \mathrm{TR}} v_i \phi_i S_i, \tag{2}$$

where i denotes a grid block, the sum is over all blocks outside the target region (TR), v_i is the bulk volume of cell i, ϕ_i

is the porosity of cell i, and S_i is the CO_2 saturation in cell i. The goal of the monitoring well optimization is to locate the monitoring wells such that the expected variance in J (over the set of N_r realizations), conditioned to the measurement data, is minimized. This acts to increase our knowledge regarding the plume extent after the 20-year time frame.

The optimization problem can be expressed as

$$\mathbf{y}_{\text{opt}} = \arg\min_{\mathbf{y}} \left[\int \int \sigma^2_{J|d_{obs}(m,y,\epsilon)} p(\mathbf{m}) p(\boldsymbol{\epsilon}) d\mathbf{m} d\boldsymbol{\epsilon} \right], \quad (3)$$

where $\mathbf{y}_{\text{opt}}$ denotes the optimum monitoring locations and $\sigma^2_{J|d_{obs}(m,y,\epsilon)}$ is the posterior variance of J, given measured data $\mathbf{d}_{obs}(\mathbf{m}, \mathbf{y}, \boldsymbol{\epsilon})$. Assuming that multivariate Gaussian statistics are preserved in the data space, Sun and Durlofsky [21] showed that the integral in Eq. 3 can be expressed as

$$\begin{aligned} &\int \int \sigma^2_{J|d_{obs}(m,y,\epsilon)} p(\mathbf{m}) p(\boldsymbol{\epsilon}) d\mathbf{m} d\boldsymbol{\epsilon} \\ &= \sigma^2_{JJ} - C_{Jd_h} (C_{d_h d_h} + C_D)^{-1} C_{d_h J}, \end{aligned} \quad (4)$$

where the covariances are determined from the simulation results over the N_r prior models. The specific computations are

$$\sigma^2_{JJ} = \frac{1}{N_r - 1} \sum_{i=1}^{N_r} (J_i - \mu_J)^2, \quad (5)$$

$$C_{Jd_h} = C^T_{d_h J} = \frac{1}{N_r - 1} \sum_{i=1}^{N_r} (J_i - \mu_J) \left[(\mathbf{d}_h)_i - \boldsymbol{\mu}_{d_h} \right], \quad (6)$$

$$C_{d_h d_h} = \frac{1}{N_r - 1} \sum_{i=1}^{N_r} \left[(\mathbf{d}_h)_i - \boldsymbol{\mu}_{d_h} \right] \left[(\mathbf{d}_h)_i - \boldsymbol{\mu}_{d_h} \right]^T, \quad (7)$$

where J_i and $(\mathbf{d}_h)_i$ represent the simulated QoI value and monitoring well data (at locations defined by $\mathbf{y}$) for prior model i. Furthermore, μ_J and $\boldsymbol{\mu}_{d_h}$ denote the prior means over the N_r models in the ensemble.

Combining Eqs. 3 and 4 gives

$$\mathbf{y}_{\text{opt}} = \arg\min_{\mathbf{y}} \left[\sigma^2_{JJ} - C_{Jd_h} (C_{d_h d_h} + C_D)^{-1} C_{d_h J} \right]. \quad (8)$$

The covariance terms depend on the monitoring well locations $\mathbf{y}$, but the variance σ^2_{JJ} does not depend on $\mathbf{y}$ because the QoI values for the prior models are not affected by the monitoring plan. This allows the optimization problem to be rewritten as

$$\mathbf{y}_{\text{opt}} = \arg\min_{\mathbf{y}} \left[1 - \frac{C_{Jd_h} (C_{d_h d_h} + C_D)^{-1} C_{d_h J}}{\sigma^2_{JJ}} \right], \quad (9)$$

where the entire fractional term can be interpreted as a measure of expected uncertainty reduction in J given the data measured at the monitoring well locations defined by $\mathbf{y}$. As discussed in [21], this overall approach is still applicable (though more approximate) in cases where the flow statistics are non-Gaussian.

The optimization problem given in Eq. 9 is solved using a genetic algorithm formulated in a Python environment. The optimization requires only prior simulation data. This means that, once the N_r prior realizations are simulated, no additional flow computations need be performed for the design of the monitoring strategy.

2.2 History matching procedure

We now describe the approach used for history matching. The observed data considered in the history matching step are those measured by the (optimized) monitoring wells. In this work, the 'true' data derive from a selected synthetic 'true' model that is consistent with the prior ensemble (but it is not one of the N_r models used for monitoring well optimization). Ensemble smoothing with multiple data assimilation (ES-MDA), introduced by Emerick & Reynolds [7], is applied. Specialized treatments such as localization are not used in this work.

In ES-MDA, at each of the N_a data assimilation steps, we apply

$$\mathbf{m}_i^{k+1} = \mathbf{m}_i^k + C^k_{md_h} (C^k_{d_h d_h} + \alpha_k C_D)^{-1} \left[\mathbf{d}^k_{pert,i} - \mathbf{d}^k_{h,i} \right], \quad (10)$$

for $i = 1, \ldots, N_r$ and $k = 1, \ldots, N_a$. Here $\mathbf{m}_i^{k+1}$ represents updated geomodel i ($\mathbf{m}_i^k$ is the model at the previous assimilation step), $\mathbf{d}^k_{h,i}$ contains the simulation results for model i at step k, and the covariance matrices $C^k_{md_h}$ and $C^k_{d_h d_h}$ are computed at each step. The vector $\mathbf{d}^k_{pert,i}$ denotes (perturbed) observation data, sampled from $\mathbf{d}^k_{pert,i} = \mathbf{d}_{obs} + \sqrt{\alpha_k} C_D^{1/2} \mathbf{z}^k_{d,i}$, where α_k is the ES-MDA inflation parameter, C_D is the data covariance, and $\mathbf{z}^k_{d,i} \sim \mathcal{N}(\mathbf{0}, I)$. In this work, we set $N_a = 4$ and $\alpha_k = 4$ at all assimilation steps.

The ES-MDA procedure requires a total of $N_r \times N_a$ simulation runs. Thus the computational demands for this step are substantial. The final set of history matched models, $\mathbf{m}_i$, $i = 1, \ldots, N_r$, generated after assimilation step 4, are used to provide predictions for any QoI. They can also be applied to evaluate or optimize storage aquifer performance under new conditions (e.g., increased injection rates, the introduction of additional injection wells).

3 Computational results

In this section, we first present the aquifer model and problem setup. The workflow described in Section 2 is then applied to two different injection scenarios. For each scenario, two different true models are considered. The first scenario (Section 3.2) involves a single injection well, while the second scenario (Section 3.3) involves two injection wells, with the second well starting injection 5 years after the first well.

3.1 Aquifer model

The models and problem setup in this work are based on the study by Okwen et al. [17]. That work entailed a feasibility assessment for a carbon storage project in central Illinois, USA, with CO_2 injected into the Mt. Simon formation. Aspects of the problem specification have been modified in this work, including the injection well location, injection rate, and simulation time frame. In our model the storage aquifer extends 16.15 km × 16.46 km areally. It is 1.14 km thick, with this thickness including the confining shale layer. The models are represented on a 40 × 40 × 40 grid, with cells of dimension 403.9 m × 411.5 m × 28.6 m. The size of the grid blocks and the level of resolution in these models are certainly less than ideal. In particular, the grid is too coarse to resolve detailed CO_2 plume evolution or complex multiphase flow physics. This is not a major concern here since our goal is to illustrate the overall methodology. In a practical application, it would be appropriate to introduce grid refinement, particularly in the region around the injection and monitoring wells. In addition, the incorporation of properly upscaled geomodels, and/or error models developed to correct for unresolved physics, would be useful.

The models contain six geological layers (one of these is the confining shale layer) and are constructed through Cartesian 'mappings' of more complex models defined on irregular grids. The topological structure of the layers defined in [17] is preserved in the mapping, though this treatment requires cells above the shale and below geological layer 6 to be deactivated. A geological realization of the system (geostatistical parameters are given below) is shown in Fig. 2. The zero-valued regions in this figure represent the inactive cells.

The initial pressure of the aquifer is 20.07 MPa at a depth of 1750 m. We specify a maximum bottom-hole pressure (BHP) for the injectors of 27.63 MPa. According to [17], the Environmental Protection Agency (EPA) stipulates that the maximum BHP of a Class VI injection well can be at most 90% of the formation fracture pressure. At the target injection depth of 1750 m for the Mt. Simon formation, this criterion corresponds to a maximum BHP of 29.14 MPa. Thus our specified maximum of 27.63 MPa is well within the acceptable range. Consistent with [17], no additional aquifer support is introduced into the models. The highest

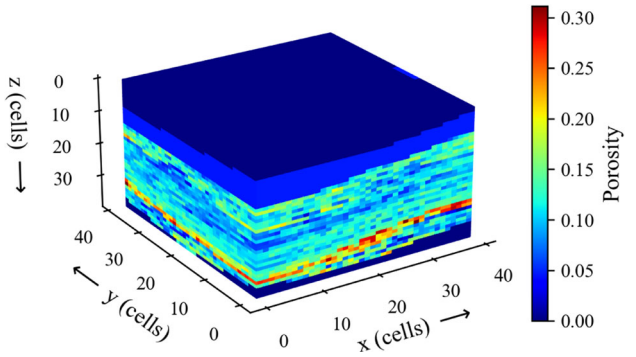

Fig. 2 Porosity field for a prior realization. The region above the confining shale layer is inactive. Vertical exaggeration applied

BHP actually reached (in all runs) remained below the specified maximum, indicating the pore volume of the models is sufficiently large for the volume of CO_2 injected.

The system is isothermal (with a temperature of 50.3°C) and initially contains only brine, of density 1150 kg/m^3. Simulations are performed using Eclipse [19] with the CO2STORE option. This simulator has preset models for the mutual solubility and fluid properties of CO_2 and brine. The gas-water relative permeability curves, which correspond to one of the scenarios considered by Okwen et al. [17], are shown in Fig. 3.

Permeability and porosity in all layers of the model, except for the confining shale layer, are taken to be uncertain. For the shale layer (layer 1), we specify a constant permeability of 0.045 md and a constant porosity of 0.046. Porosity and log-permeability realizations for the other five layers are generated through application of Gaussian sequential simulation. Realizations are constructed independently for each geological layer using the SGeMS toolbox [18]. The geological layers are then stacked to create the full realization. We proceed in this manner because the layers are geologically distinct and are characterized by different statistical distributions.

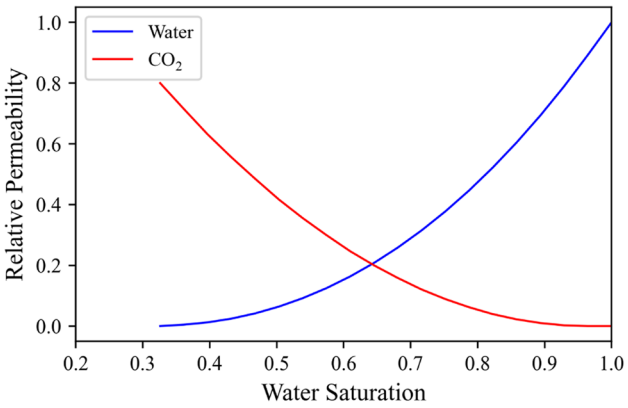

Fig. 3 Relative permeability curves for CO_2 and brine

The mean (μ) and standard deviation (σ) for the log-permeability and porosity in each layer are provided in Table 1. The models are all generated using an ellipsoid-shaped exponential variogram model. The correlation lengths in the x, y, and z-directions (l_x, l_y, l_z) for each layer are also given in Table 1. Consistent with the actual modeling of this formation, we specify $k_x = k_y$ and $k_z = 0.12k_x$ for all cells. A total of $N_r = 350$ prior geological models are constructed. Two prior realizations are shown in Fig. 4 ($\log_e k_x$ for x-z cross sections is displayed).

The geomodels are not conditioned to hard data at the well locations. Although it would be appropriate to introduce this conditioning in practice (after accounting for the difference in scale between the hard data and the grid blocks), it is somewhat involved to do this within the context of this study. This is because we will consider several different monitoring well configurations, which means the conditioning would be different in each case. This would complicate both the workflow and the comparisons between the different monitoring well strategies.

3.2 Injection scenario 1

In the first injection scenario, we consider a single vertical well, located in the center of the model. This well injects at a rate of 2.0 Mt/yr of CO_2 over a 20-year period. The injection well is perforated in the two lowermost cells in geological layer 4, in the two cells in geological layer 5, and in the uppermost cell of layer 6. As noted earlier, in all simulation runs (for prior and posterior realizations and true models), the injection-well BHP never exceeds the maximum allowable value of 27.63 MPa, indicating that pressure buildup remains within an acceptable range.

Any number of wells can be considered for monitoring, though economic considerations will limit their number in practice. Here we consider two vertical monitoring wells. These wells are assumed to measure saturation at every cell along their depth once per year, as well as pressure at three depths every 3 months. The optimization variables thus include, for each well, an x (i) location, a y (j) location, and three vertical (k) pressure transducer locations (thus $N_y = 10$).

The QoI J, for which we seek to minimize posterior uncertainty, is the CO_2 volume beyond the cells forming a $7 \times 7 \times 5$ target region centered around the injection well perforations. In qualitative terms, we wish to find the monitoring well locations that best quantify (after history matching) the volume of CO_2 that is outside this region after 20 years of injection. The target region is shown in gray in Fig. 5. To compute the objective function, we apply Eq. 2 for each realization. The goal of the monitoring well optimization is to minimize the variance of J over all N_r realizations.

A genetic algorithm, with a population of 100 individuals, is used for the optimization defined in Eq. 9. The optimization proceeds for 150 generations (iterations). The resulting optimum locations for the two monitoring wells are shown in Fig. 5 (the injection well location is also displayed). The optimization leads to a remaining variance of 0.0709. This value corresponds to the argument of Eq. 9 evaluated for the optimal monitoring well configuration. Note that the monitoring wells are located in blocks adjacent to the injector. The pressure transducers are placed above and below the injector perforations.

We will compare the performance of the optimal monitoring scheme shown in Fig. 5 to that of other (heuristic) monitoring well configurations. Three such qualitative configurations are considered. These cases are displayed in Fig. 6 along with the injection well and optimal monitoring well locations.

In Case 1, the monitoring wells are placed where the variance in the prior results is a maximum. Here variance is computed in both saturation and pressure for each cell at each time step, over all $N_r = 350$ prior simulation runs. The normalized pressure and saturation variances are combined with equal weighting. The (i, j) locations for the monitoring wells, along with the corresponding depths for the pressure transducers, are then determined such that the variance is maximized. In the case of two or more monitoring wells, this procedure is repeated to find the next (i, j) location and corresponding depths. Note that this approach, although quantitative in character, does not account for the specific QoI (J). In Cases 2 and 3, the monitoring wells are located just outside the target region, in different configurations. For these cases, the pressure transducer depths are taken to be the same as in the optimal configuration.

We can directly evaluate the argument of Eq. 9 for each of the three heuristic cases. The remaining variance is, for Cases 1–3, 0.0784, 0.6912, 0.6508, respectively. These values are all greater than that for the optimum configuration (0.0709), though Case 1 (based on prior variance) is comparable to the optimum. We might thus expect this configuration

Table 1 Geostatistical parameters for each geological layer

Layer	μ_ϕ	σ_ϕ	$\mu_{\log k}$	$\sigma_{\log k}$	l_x	l_y	l_z
2	0.117	0.039	2.223	2.332	24	24	4
3	0.096	0.018	1.061	2.631	21	22	3
4	0.102	0.016	1.690	1.173	29	30	4
5	0.215	0.040	4.641	1.994	26	23	1
6	0.123	0.043	2.540	2.667	25	24	2

Layer 1 (shale layer) is not shown because these properties do not vary. Log properties are $\log_e k_x$ in md. Correlation lengths are in number of grid blocks in the corresponding direction. Mean values for each layer are from [17]

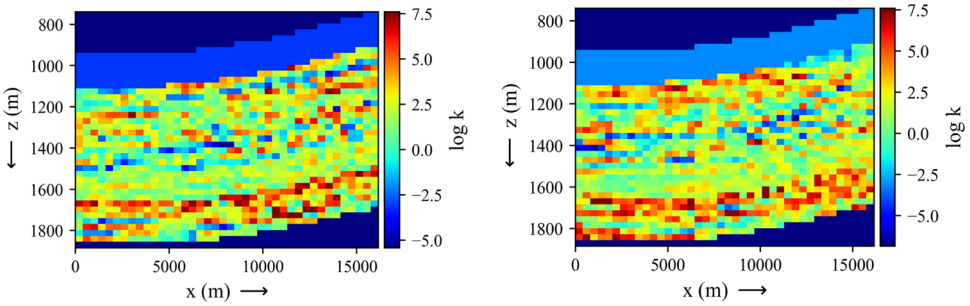

(a) Realization 2

(b) Realization 214

Fig. 4 Two prior realizations of log-permeability for x-z cross sections

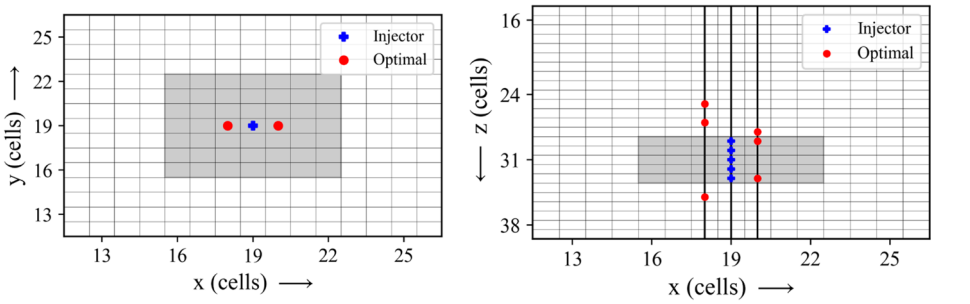

(a) Top view of optimum monitoring wells

(b) Cross-sectional view of optimum monitoring wells

Fig. 5 Optimal monitoring well configuration. Injection well location and perforations also shown (injection scenario 1). Gray shaded blocks indicate target region

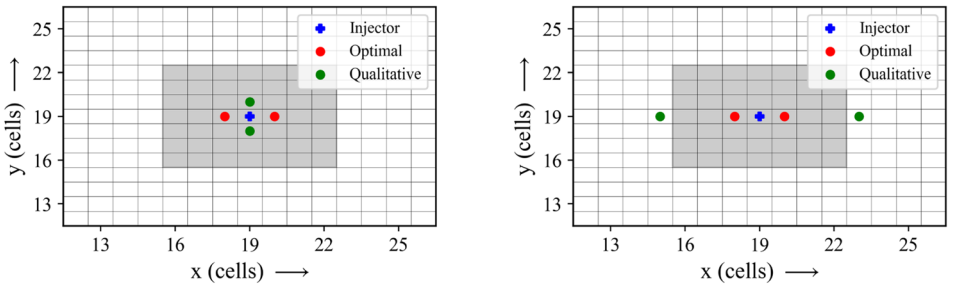

(a) Case 1 – monitoring wells where variance in the prior results is maximum

(b) Case 2 – monitoring wells on either side of the target region

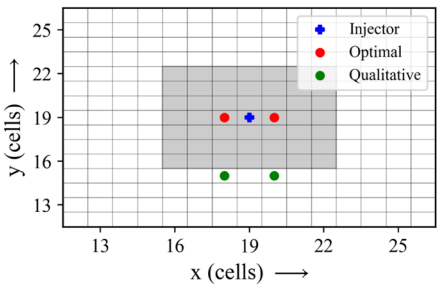

(c) Case 3 – monitoring wells near one another outside the target region

Fig. 6 Monitoring well locations for various qualitative (heuristic) schemes. Optimal configuration and injection well also shown (injection scenario 1). Gray shaded blocks indicate target region

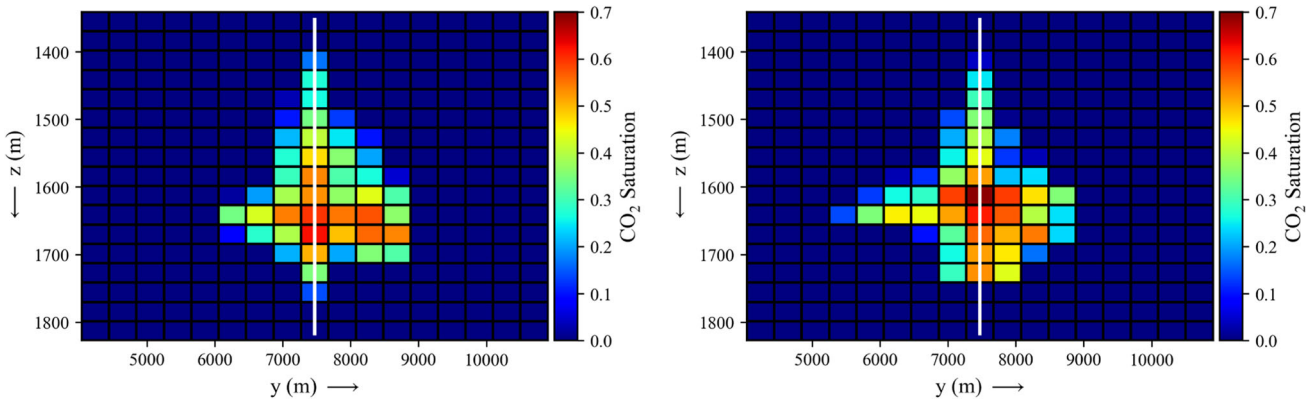

(a) True model 1 (b) True model 2

Fig. 7 Cross-sectional view of CO_2 plume (along $x = 19$) after 20 years of injection for both true models (injection scenario 1). White line indicates the injection well

to perform better than the other two cases in terms of the uncertainty reduction achieved via history matching.

We now apply history matching using the data provided by the monitoring wells over the 20-year injection period. As this study involves synthetic models, the data here derive from the simulation of a 'true' model. This model is a new geological realization that is consistent with the prior ensemble but was not included in the monitoring well optimization. We will consider two such true models (in turn).

ES-MDA is applied (separately) using data from the optimal monitoring scheme and from each of the three heuristic monitoring scenarios. A cross-sectional y-z view (through $x = 19$, where x here refers to the grid index) of the CO_2 plume for true model 1, after 20 years of injection, is shown in Fig. 7a. Note that this cross-section contains the injector, which is indicated in the figure.

After performing history matching using observed data from true model 1, the volume of CO_2 beyond the target region for each of the 350 posterior models is computed. Empirical cumulative distribution functions (CDFs) for this quantity, computed over the 350 posterior models for each monitoring scheme, are shown in Fig. 8a. The dashed vertical line (at a J value of 3.27×10^6 m^3) indicates the true-model result. The red curve depicts the prior CDF (before any data assimilation is performed). The blue curve shows the posterior CDF for the optimal monitoring well configuration, and the other curves correspond to the qualitative monitoring scenarios.

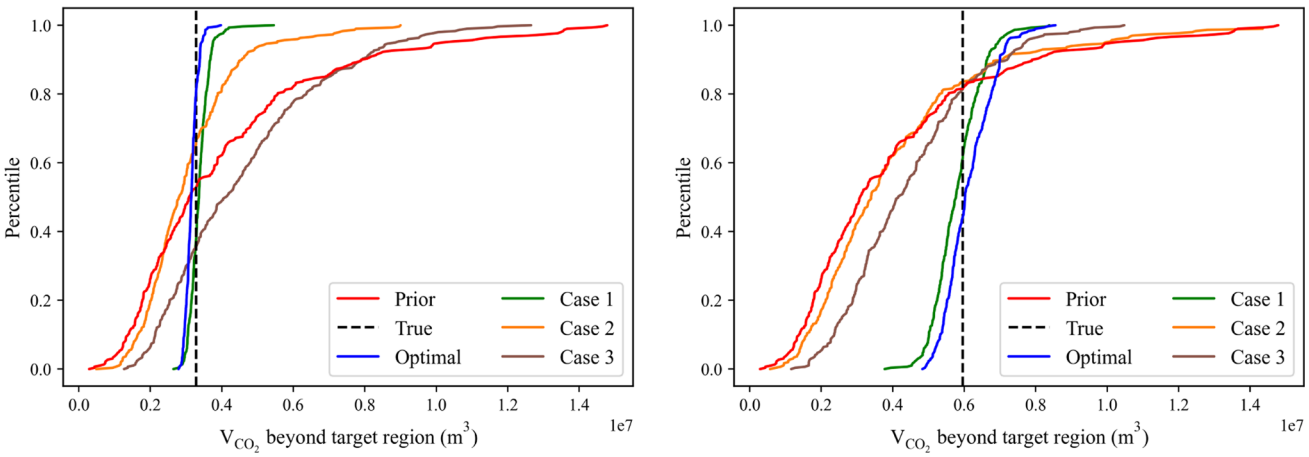

(a) True model 1 (b) True model 2

Fig. 8 CDFs for CO_2 volume beyond the target region (J). The red curve is the prior, blue curve is the posterior for the optimal monitoring scheme, and the other solid curves are posteriors for heuristic monitoring schemes. The vertical dashed line is the J value for the corresponding true model (injection scenario 1)

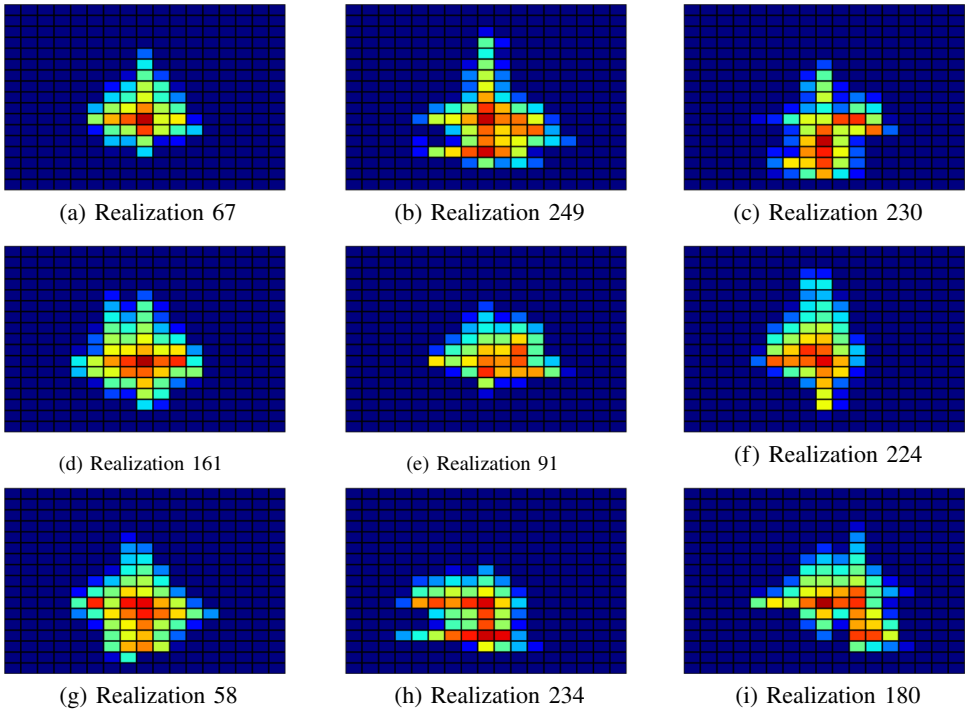

Fig. 9 CO_2 plumes in $x = 19$ cross-section after 20 years of injection for nine randomly chosen prior realizations (injection scenario 1)

(a) Realization 67 (b) Realization 249 (c) Realization 230

(d) Realization 161 (e) Realization 91 (f) Realization 224

(g) Realization 58 (h) Realization 234 (i) Realization 180

In this figure, the width of each CDF corresponds to the degree of uncertainty in J. The prior is very broad, indicating high initial uncertainty. We see that the blue curve, which depicts the CDF for the posterior of J after history matching using data from the optimum monitoring well configuration, is relatively narrow and is centered around the true result. This is precisely as desired, and indicates that the history matching has successfully reduced uncertainty in the quantity of interest (J). In Fig. 8a we also see that the heuristic scheme based on prior variance (Case 1) leads to a posterior CDF that is close to that for the optimum configuration. The other cases provide less uncertainty reduction. This illustrates the strong

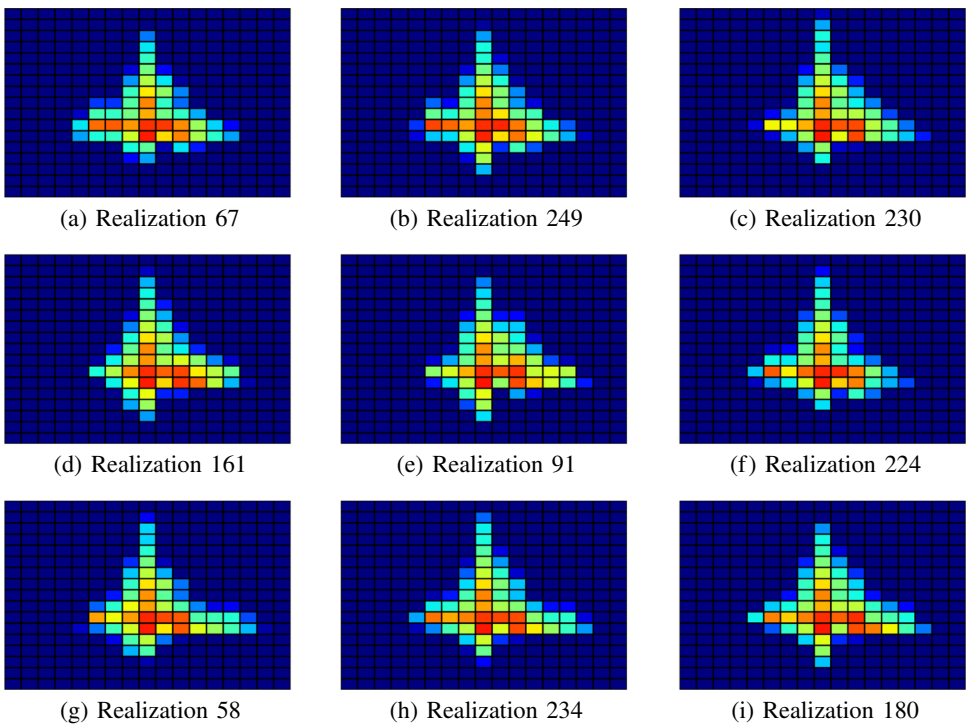

Fig. 10 CO_2 plumes in $x = 19$ cross-section after 20 years of injection for nine posterior realizations. Observed data are from the optimum monitoring well configuration (true model 1, injection scenario 1)

(a) Realization 67 (b) Realization 249 (c) Realization 230

(d) Realization 161 (e) Realization 91 (f) Realization 224

(g) Realization 58 (h) Realization 234 (i) Realization 180

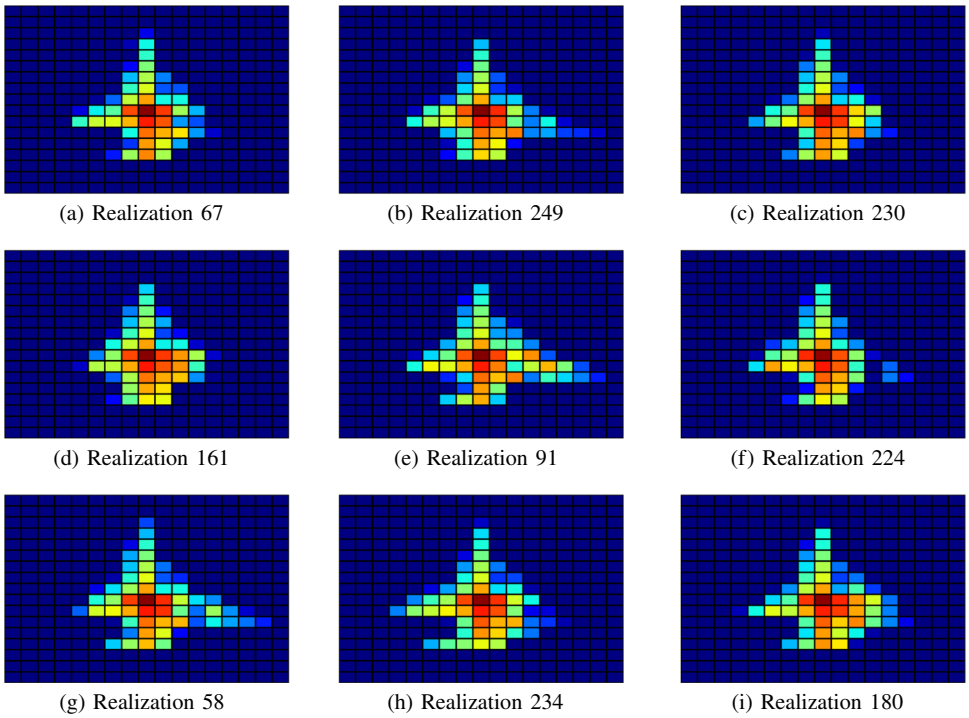

(a) Realization 67 (b) Realization 249 (c) Realization 230

(d) Realization 161 (e) Realization 91 (f) Realization 224

(g) Realization 58 (h) Realization 234 (i) Realization 180

Fig. 11 CO_2 plumes in $x = 19$ cross-section after 20 years of injection for nine posterior realizations. Observed data are from the optimum monitoring well configuration (true model 2, injection scenario 1)

effect that the locations of the monitoring wells have on the quality of posterior predictions.

We next consider prior and posterior simulation results for CO_2 plume location. This is an essential quantity in any data assimilation workflow in a CCUS setting. Figure 9 displays the CO_2 plume saturations after 20 years of injection for nine randomly selected prior realizations. These figures again correspond to cross-sections through $x = 19$, as in Fig. 7a.There is clear variability in the shape and extent (vertical and lateral) of these plumes, consistent with the broad prior CDF in Fig. 8a. Plumes corresponding to posterior models are shown in Fig. 10. These plumes are clearly more consistent in size and shape than those in Fig. 9. More importantly, they are visually similar to the true-model plume shown in Fig. 7a.

We now present posterior results for a different true model. Note that the monitoring well optimization and associated simulations do not need to be repeated, as these involve only prior models and no observed data. The CO_2 plume saturation for true model 2 is shown in Fig. 7b. The prior and posterior CDFs for this case are presented in Fig. 8b. Note that the true J value is now larger than it was for true model 1 (here it corresponds to the 81st percentile on the prior CDF compared to the 52nd percentile for true model 1). For this true model, the optimal monitoring well configuration clearly provides the most uncertainty reduction. Of the heuristic monitoring schemes, Case 1 again performs the best. The CO_2 plumes for the posterior models, for the optimal monitoring well scenario, are shown in Fig. 11. These plumes again resemble the true-model result (Fig. 7b) and they display less variation than the plumes corresponding to prior realizations shown in Fig. 9.

The application of ES-MDA provides an ensemble ($N_r = 350$) of posterior geomodels and corresponding simulation results. These results can be used to provide possible future plume migration scenarios conditioned to the data measured at the monitoring wells. As an example, time-evolution results for a particular posterior realization from the true model 2 example, with data collected at optimally located monitoring wells, are displayed in Fig. 12. In this case, we continue injecting CO_2 for an additional 30 years. The saturation field is again for the $x = 19$ cross-section.

From the full history matched ensemble we can compute, e.g., average behavior, the expected lateral extent of the plume, the probability that the plume will migrate a specific distance in a particular direction at a given time, etc. Thus these results can be very useful for aquifer management and risk assessment.

3.3 Injection scenario 2

We now consider a second injection scenario. A more limited set of results will be presented for this scenario than for injection scenario 1, as the goal here is to illustrate the

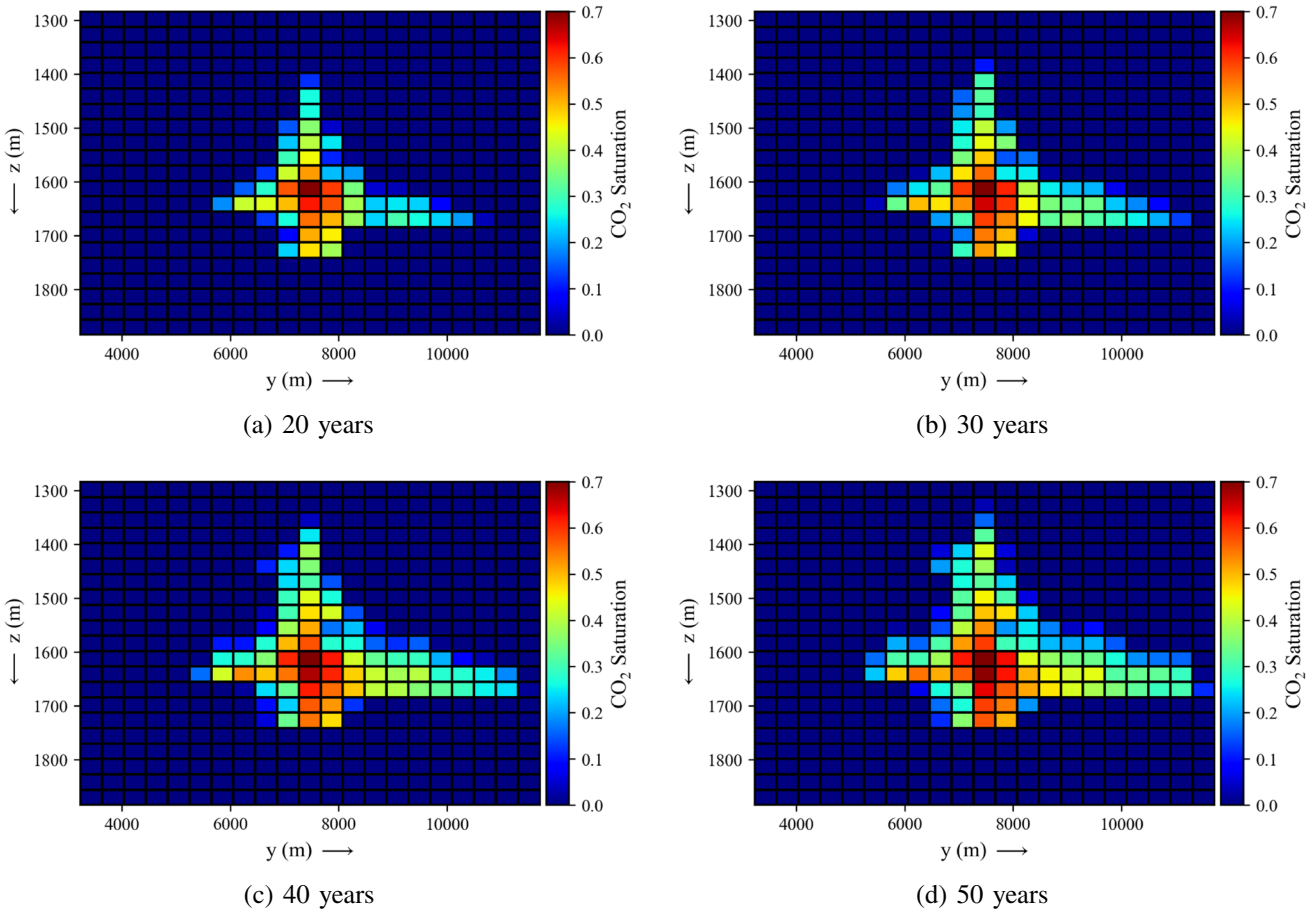

(a) 20 years (b) 30 years

(c) 40 years (d) 50 years

Fig. 12 CO_2 plumes in $x = 19$ cross-section for posterior realization 42 at later times. CO_2 is injected in this case for 50 years. Observed data are from the optimum monitoring well configuration (true model 2, injection scenario 1)

Fig. 13 CO_2 plumes in $x = 19$ cross-section after 20 years of injection for nine randomly chosen prior realizations (injection scenario 2)

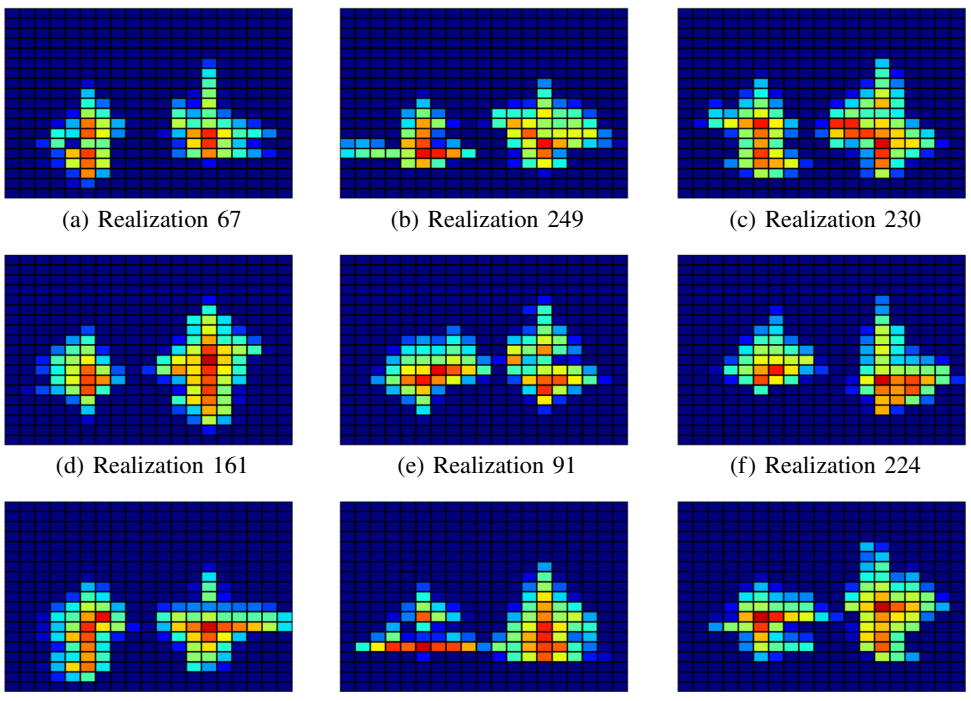

(a) Realization 67 (b) Realization 249 (c) Realization 230

(d) Realization 161 (e) Realization 91 (f) Realization 224

(g) Realization 58 (h) Realization 234 (i) Realization 180

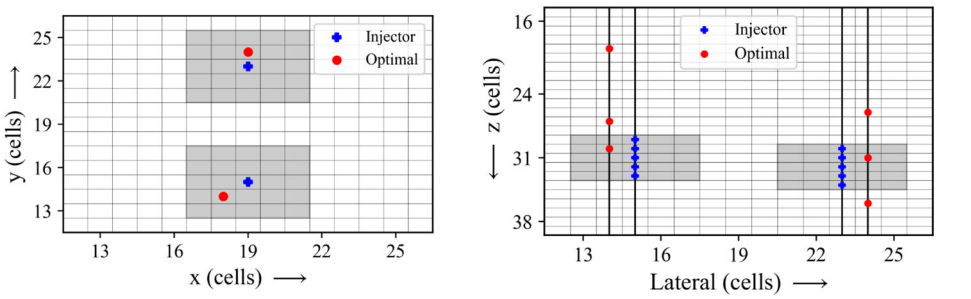

Fig. 14 Optimal monitoring well configuration. Injection well location and perforations also shown (injection scenario 2). Gray shaded blocks indicate target region

(a) Top view of optimum monitoring wells

(b) Conceptual cross-sectional view of optimum monitoring wells

applicability of the framework in a range of settings. This scenario involves two vertical injection wells, with both wells injecting 2.0 Mt CO_2/yr. The first injector operates at this rate for the full 20-year period, while the second begins injection after 5 years. The maximum injection-well BHP is specified as 27.63 MPa for each well (this is the same value used in injection scenario 1).

We again consider a strategy with two vertical monitoring wells, each with three pressure transducers. Pressure data at each transducer are collected every three months and saturation data are measured once per year along the well (at each grid block). The objective function, J, is analogous to that used for injection scenario 1. In this case it is defined as the CO_2 volume beyond $n \times n \times n_p$ regions around the perforated portion of each injector. Here we set $n = 5$. The target region now entails all gray-shaded blocks in Fig. 13.

The prior flow simulations must be rerun, as the injector locations and rate schedules are different in this scenario. The setup is otherwise identical to that described in Section 3.2. Prior flow simulation results for nine realizations are shown in Fig. 13. The two separate plumes for this case are clearly evident. The monitoring optimization is also rerun, again with the same specifications as were used previously.

The optimized monitoring well locations, along with the injection wells, are displayed in Fig. 14. The monitoring wells are placed close to each of the injectors. In injection scenario 1, the optimal monitoring wells were aligned with the y-axis (Fig. 5a), which allowed for direct visualization of the pressure transducer depths (Fig. 5b). However, for this injection scenario, the monitoring wells are not aligned along either the x or y axis (as is evident in Fig. 14a). Therefore, in order to display the pressure transducers, we plot them in Fig. 14b along a 'conceptual' cross section that runs through both injectors and both monitoring wells. For this optimized plan, the remaining variance corresponding to the argument in Eq. 9 is 0.2351. Note that this value is larger than in injection scenario 1 (where it was 0.0709), which is

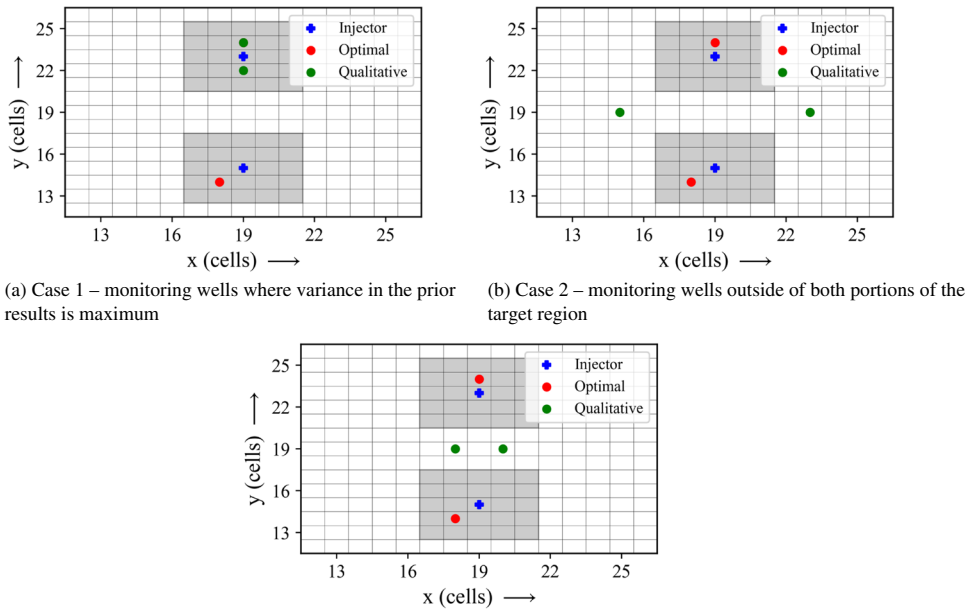

Fig. 15 Monitoring well locations for various qualitative (heuristic) schemes. Optimal configuration and injection wells also shown (injection scenario 2). Gray shaded blocks indicate target region

(a) Case 1 – monitoring wells where variance in the prior results is maximum

(b) Case 2 – monitoring wells outside of both portions of the target region

(c) Case 3 – monitoring wells between the two portions of the target region

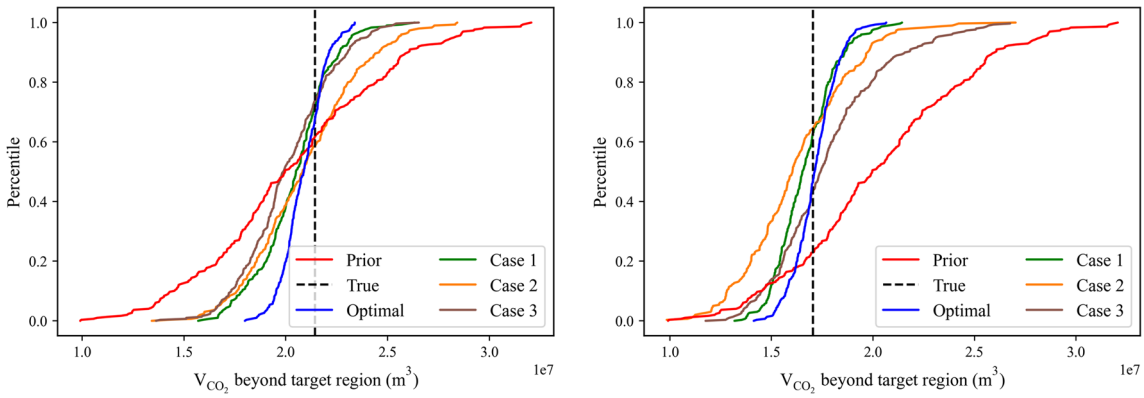

(a) True model 1

(b) True model 2

Fig. 16 CDFs for CO_2 volume beyond the target region (J). The red curve is the prior, blue curve is the posterior for the optimal monitoring scheme, and the other solid curves are posteriors for heuristic monitoring schemes. The vertical dashed line is the J value for the corresponding true model (injection scenario 2)

likely due to the added complexity from having two injection wells rather than one.

Three heuristic monitoring plans are again considered. These are shown, along with the injection wells and optimal monitoring well locations, in Fig. 15. Case 1 again corresponds to placing monitoring wells where the variance in the prior results is the largest. In this case the monitoring wells are both positioned near one injection well (the well that begins injecting at the start of the operation).

For Cases 2 and 3, the x-y locations for the monitoring wells are shifted relative to the optimum, but the vertical locations of the pressure transducers are the same as in the optimum strategy. The remaining variance (from Eq. 9) for Case 1 is 0.3512, which is further from the optimal value than in injection scenario 1. For Cases 2 and 3, the remaining variance is larger, 0.6128 and 0.5023, respectively.

We now present posterior results for the same two true models as were used in Section 3.2. For each true model and monitoring scheme, ES-MDA is applied with data collected over the 20-year period. Results for the different monitoring schemes are shown in Fig. 16. The curves are as described earlier, and the dashed line denotes the true value. Note that the J values are consistently larger here than in injection scenario 1. This is due to the additional 2.0 Mt CO_2/yr injected into the system (starting after 5 years), and also to the smaller target region around each injector (5×5 areally versus 7×7).

For true model 1 (Fig. 16a), all of the monitoring schemes achieve a reasonable degree of uncertainty reduction, though the optimal scheme clearly provides the most narrow posterior CDF. There is more difference between the optimal scheme and Case 1 for this injection scenario than for injection scenario 1 (compare Figs. 16a and 8a). For true model 2 (Fig. 16b), the optimal strategy again outperforms the other monitoring schemes. The Case 1 posterior CDF is close to the optimal, while the other two heuristic strategies show larger differences. Note that true model 2 corresponds to a lower percentile on the prior CDF for J than true model 1 for this injection scenario. This is in contrast to injection scenario 1 (Fig. 8).

3.4 Comparison of posterior variance assessments

As discussed in Section 2.1, the monitoring optimization strategy used in this study is strictly applicable when the simulated flow data follow multi-Gaussian distributions. The data for complex, nonlinear multiphase flow systems do not, however, follow this distribution, even if the input geomod-

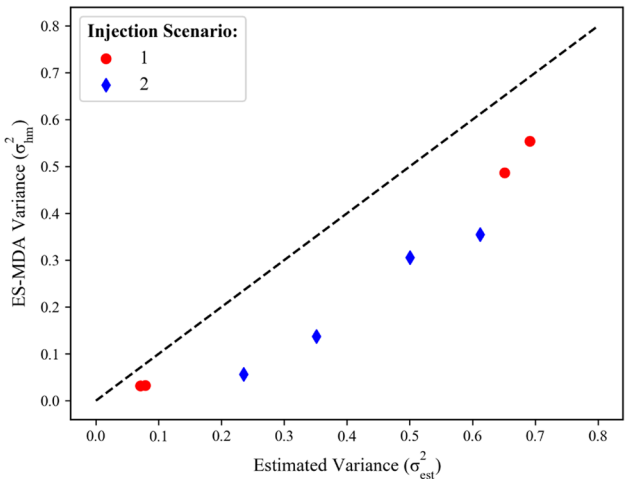

Fig. 17 Cross-plot of posterior variance in J in the history matched models versus estimated posterior variance in J under Gaussian-data assumption, for both injection scenarios and all monitoring schemes. The σ^2_{hm} results are averages over true models 1 and 2. The 45° line is also shown

els are themselves multi-Gaussian. Thus, it is of interest to compare the actual uncertainty reduction achieved through ES-MDA-based history matching to that estimated from the argument of Eq. 9. This assessment can be performed for the various monitoring schemes and injection scenarios. One caveat is that Eq. 9 provides an estimate over all possible true models (assuming the prior ensemble is representative), while the history matching results in this study involve only two different true models.

In Fig. 17, we present a cross-plot between the estimated posterior variance in J (from Eq. 9), denoted σ^2_{est}, and the posterior variance in J actually observed in the history matched models, denoted σ^2_{hm}. Here σ^2_{hm} is the average of the results for true models 1 and 2. Results are displayed for all monitoring schemes with both injection scenarios. Two notable features are evident. First, the trend/ordering is consistent between the two sets of results. This suggests that different monitoring strategies can be (at least approximately) ranked by evaluating σ^2_{est}, which is useful because the computation of σ^2_{est} requires only prior-model simulations (not history matching). The second observation is that the history matched results consistently lie below the 45° line. This is consistent with theory, since the Gaussian estimate is known to provide an upper bound for posterior variance in cases where the data are non-Gaussian [21]. It is also possible that some of this discrepancy is due to the under-estimation of posterior uncertainty by ES-MDA. This effect, particularly in the absence of localization, has been discussed in previous studies (e.g., [15]) and may be occurring in our results. A full understanding of the shift evident in Fig. 17 will, however, require further investigation.

4 Concluding remarks

In this study, we presented a framework for optimally monitoring and history matching a CO_2 storage project. The workflow involves the determination of the optimal monitoring well locations based on simulations of prior realizations, followed by the application of history matching as data are collected. The monitoring well optimization step is essentially that presented in [21], though history matching here is performed in a model-based (rather than data-space) setting using ES-MDA. The framework was applied to a system representative of a CO_2 storage project under study for the Mt. Simon formation in Illinois, USA. An efficient remapping algorithm was used to represent the underlying unstructured model on a coarser Cartesian grid.

Results were presented for two different injection scenarios and two true models. In the first injection scenario, a single well operated for a 20-year period, while the second scenario involved two CO_2 injectors. The true models in each case were consistent with the prior ensemble and provided the (synthetic) observations used for data assimilation. History matching using data from optimally located monitoring wells was shown to provide more uncertainty reduction than was achieved using heuristic monitoring plans, though the advantage was relatively slight in some cases.

In contrast to the data-space approach in [21], the workflow here provides an ensemble of posterior models. These can be used to assess average or outlier plume evolution scenarios, analyze commonalities and differences in history matched geomodels, etc.

There are many directions that should be pursued in future work in this area. The models in this study were defined on 40 $\times$ 40 $\times$ 40 grids. Models of these dimensions are too coarse to resolve detailed CO_2 saturation distributions, so higher grid resolution will be required in practice. This could be achieved through use of locally refined models, with high resolution near injection and monitoring wells. Error modeling procedures, in which errors due to grid resolution are quantified based on simulation results from selected pairs of fine and coarse-scale models, could also be effective. The use of deep-learning-based surrogate models, such as those described in [23, 24], should also be considered. The impact of additional monitoring wells, and/or the effect of measuring data more frequently, should be studied. This could be treated in a multiobjective optimization setting where the objectives are to maximize uncertainty reduction while minimizing monitoring cost. Other data types, particularly geophysical measurements, could be included in the history matching step. Additional physics, such as geomechanical effects, can be incorporated into the overall workflow. Finally, the methodology should be generalized to optimize new monitoring wells placed after the start of CO_2 injection.

Acknowledgements We thank Oleg Volkov for his assistance with computational resources, Su Jiang for providing ES-MDA code, David Cameron for useful discussions, Steven Whittaker for project management, Roland Okwen and Yang Fang for assistance with the geomodels and simulations, and Nathan Grigsby for geological data. We also acknowledge the Stanford Center for Computational Earth & Environmental Science for providing the computational resources used in this study.

Funding This work was funded by the U.S. Department of Energy under project DE-FE0031892. Additional support was provided by the Stanford Center for Carbon Storage and Stanford Smart Fields Consortium.

Declarations

Conflicts of interest The authors declare that they have no known competing financial interests or personal relationships that could have appeared to influence the work reported in this paper

References

1. Ayani, M., Grana, D., Liu, M.: Stochastic inversion method of time-lapse controlled source electromagnetic data for CO_2 plume monitoring. Int. J. Greenhouse Gas Control **100**, 103098 (2020)
2. Barros, E., Leeuwenburgh, O., Szklarz, S.: Quantitative assessment of monitoring strategies for conformance verification of CO_2 storage projects. Int. J. Greenhouse Gas Control **110**, 103403 (2021)
3. Cameron, D.A., Durlofsky, L.J.: Optimization and data assimilation for geological carbon storage. Computational models for CO_2 sequestration and compressed air energy storage, R. Al-Khoury and J. Bundschuh, eds., Taylor & Francis Group/CRC Press pp. 357–388 (2014)
4. Cameron, D.A., Durlofsky, L.J., Benson, S.M.: Use of above-zone pressure data to locate and quantify leaks during carbon storage operations. Int. J. Greenhouse Gas Control **52**, 32–43 (2016)
5. Chen, B., Harp, D.R., Lin, Y., Keating, E.H., Pawar, R.J.: Geologic CO_2 sequestration monitoring design: a machine learning and uncertainty quantification based approach. Appl. Energy **225**, 332–345 (2018)
6. Chen, B., Harp, D.R., Lu, Z., Pawar, R.J.: Reducing uncertainty in geologic CO_2 sequestration risk assessment by assimilating monitoring data. Int. J. Greenhouse Gas Control **94**, 102926 (2020)
7. Emerick, A.A., Reynolds, A.C.: Ensemble smoother with multiple data assimilation. Comput. Geosci. **55**, 3–15 (2013)
8. Finley, R.J., Frailey, S.M., Leetaru, H.E., Senel, O., Couëslan, M.L., Scott, M.: Early operational experience at a one-million tonne CCS demonstration project, Decatur, Illinois, USA. Energy Proced. **37**, 6149–6155 (2013)
9. Furre, A.K., Eiken, O., Alnes, H., Vevatne, J.N., Kiær, A.F.: 20 years of monitoring CO_2-injection at Sleipner. Energy Proced. **114**, 3916–3926 (2017)
10. González-Nicolás, A., Baù, D., Alzraiee, A.: Detection of potential leakage pathways from geological carbon storage by fluid pressure data assimilation. Adv. Water Resources **86**, 366–384 (2015)
11. González-Nicolás, A., Cihan, A., Petrusak, R., Zhou, Q., Trautz, R., Riestenberg, D., Godec, M., Birkholzer, J.T.: Pressure management via brine extraction in geological CO_2 storage: adaptive optimization strategies under poorly characterized reservoir conditions. Int. J. Greenhouse Gas Control **83**, 176–185 (2019)
12. He, X., Zhu, W., Santoso, R., Alsinan, M., Kwak, H., Hoteit, H.: CO_2 leakage rate forecasting using optimized deep learning. In: SPE Annual Technical Conference and Exhibition. OnePetro (2021)
13. Jenkins, C.: The state of the art in monitoring and verification: an update five years on. Int. J. Greenhouse Gas Control **100**, 103118 (2020)
14. Jeong, H., Sun, A.Y., Zhang, X.: Cost-optimal design of pressure-based monitoring networks for carbon sequestration projects, with consideration of geological uncertainty. Int. J. Greenhouse Gas Control **71**, 278–292 (2018)
15. Lacerda, J.M., Emerick, A.A., Pires, A.P.: Using a machine learning proxy for localization in ensemble data assimilation. Computat. Geosci. **25**, 931–944 (2021)
16. Liu, M., Grana, D.: Petrophysical characterization of deep saline aquifers for CO_2 storage using ensemble smoother and deep convolutional autoencoder. Adv. Water Resources **142**, 103634 (2020)
17. Okwen, R., Babrinde, O., Taft, K.: Storage complex modeling for CarbonSAFE Illinois – Macon county. Tech. Rep., Univ. of Illinois at Urbana-Champaign, IL (United States) (2022)
18. Remy, N., Boucher, A., Wu, J.: Applied geostatistics with SGeMS: a User's guide. Cambridge University Press (2009)
19. Schlumberger: Eclipse reference manual, 2017.2 edn. (2017)
20. Strandli, C.W., Mehnert, E., Benson, S.M.: CO_2 plume tracking and history matching using multilevel pressure monitoring at the Illinois Basin-Decatur project. Energy Proc. **63**, 4473–4484 (2014)
21. Sun, W., Durlofsky, L.J.: Data-space approaches for uncertainty quantification of CO_2 plume location in geological carbon storage. Adv. Water Resources **123**, 234–255 (2019)
22. Tadjer, A., Bratvold, R.B.: Managing uncertainty in geological CO_2 storage using Bayesian evidential learning. Energies **14**(6), 1557 (2021)
23. Tang, M., Ju, X., Durlofsky, L.J.: Deep-learning-based coupled flow-geomechanics surrogate model for CO_2 sequestration. Int. J. Greenhouse Gas Control **118**, 103692 (2022)
24. Wen, G., Hay, C., Benson, S.M.: CCSNet: a deep learning modeling suite for CO_2 storage. Adv. Water Resources **155**, 104009 (2021)
25. Yang, Y.M., Dilmore, R., Mansoor, K., Carroll, S., Bromhal, G., Small, M.: Risk-based monitoring network design for geologic carbon storage sites. Energy Proc. **114**, 4345–4356 (2017)
26. Yang, Y.M., Dilmore, R.M., Bromhal, G.S., Small, M.J.: Toward an adaptive monitoring design for leakage risk - closing the loop of monitoring and modeling. Int. J. Greenhouse Gas Control **76**, 125–141 (2018)
27. Zou, A., Durlofsky, L.J.: Integrated framework for optimization of horizontal/deviated well placement and control for geological CO_2 storage. In: SPE Reservoir Simulation Conference. OnePetro (2023)